

Interannual variations in snow melt over Arctic sea ice and relationships to atmospheric forcings

MARK C. SERREZE, JAMES A. MASLANIK, GREGORY R. SCHARFEN, ROGER G. BARRY
*Division of Cryospheric and Polar Processes, Cooperative Institute for Research in Environmental Sciences,
University of Colorado, Boulder, CO80309-0449, U.S.A.*

DAVID A. ROBINSON
Department of Geography, Rutgers University, Kilmer Campus, Piscataway, NJ 08854, U.S.A.

ABSTRACT. Spring snow melt over the Beaufort and East Siberian seas is examined using visible-band DMSP imagery, SMMR brightness temperatures, and surface air temperatures for the years 1979, 1980 and 1984–86. Regional melt onset, as identified from the SMMR data, typically begins in early June, but can vary by up to two weeks between years. The subsequent pace of melt, estimated from the difference in days between the SMMR signal and visual identification of melt features in the DMSP data, exhibits a similar range. Interannual differences in snow melt are examined with respect to variations in cloud cover and geostrophic meridional winds. While over the Beaufort Sea, early melt onset and rapid melt progression may be favored by a combination of limited cloud cover and, as inferred from the wind data, strong northward air advection, no firm conclusions can be drawn from the available data. Presumably, potential relationships between melt and atmospheric forcings tend to be masked by additional factors, such as variations in initial snow depth and uncertainties in the data sets.

INTRODUCTION

Variations in spring snow melt over Arctic sea ice may strongly impact Arctic surface net radiation budgets by influencing surface albedo (Barry and others, 1989). Limited information exists, however, concerning inter-annual variations in snow melt and whether such variations can be differentiated with respect to forcings of cloud cover and advection (Scharfen and others, 1987; Serreze and others, 1991; Robinson and others, 1992).

Factors controlling the timing of snow melt are likely to be complex. As by May the potential solar flux to the surface is large, it seems intuitive that limited cloud cover, by itself, will result in rapid decay of the snowpack. However, extensive cloudiness augments the downwelling longwave flux, and when surface albedo is high (e.g. 70%), surface net radiation under cloudy conditions may actually be greater than under clear skies (cf. Ambach, 1974; Wendler, 1986). This suggests that cloudy conditions might hasten the seasonal increase in air and snow temperatures, allowing for earlier initial ripening of the snowpack.

Melt should also be influenced by atmospheric advection. While strong on-ice (northward) airflows should favor early melt, at least near coastal regions (e.g. Serreze and others, 1991), the extensive stratus that characterizes the Arctic Ocean during spring and summer is also related to low-level advection (Curry and Herman, 1985), such that on-ice winds may in turn give rise to

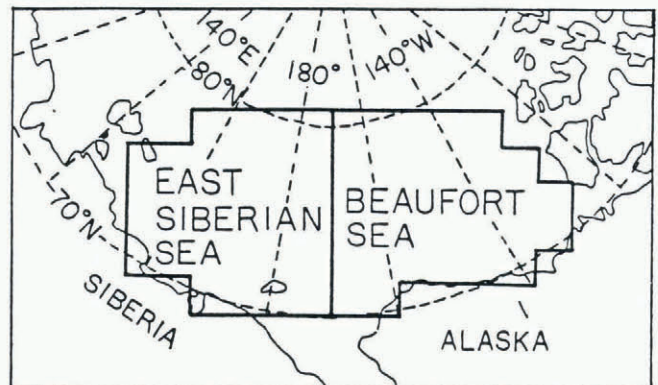


Fig. 1. Location map of the Arctic showing the two study areas: (1) Beaufort Sea, (2) East Siberian Sea.

more extensive cloud cover. Although the decrease in the absorbed solar flux may mitigate the effects of advection, this again might be offset by the corresponding increase in the downwelling longwave radiation component.

In this paper, three data sets are used to estimate the date of snow melt onset and its subsequent progression in the Beaufort and East Siberian seas (Fig. 1) for the years 1979, 1980, 1984–86. Possible atmospheric controls on variations in snow melt are then addressed through examination of regional variations in satellite-derived

cloud cover, meridional geostrophic winds, and surface air temperatures.

DATA SOURCES

Snow melt

The first snow-melt data source is based on 37 GHz vertically polarized brightness temperatures from the Nimbus-7 Scanning Multichannel Microwave Radiometer (SMMR). During spring, there is a gradual increase in SMMR brightness temperatures due to increasing physical temperature of the snow surface, usually followed by an abrupt increase often in excess of 20 K. This "jump" is consistent with the effects on microwave emissivity of a small amount (typically 1%) of liquid water in the snowpack, which identifies a date of the earliest initiation of snow melt (Anderson, 1987; Maslanik and Barry, 1989), defined here as $Date_{SMMR}$. Here, we extract and average brightness temperatures for all pixels with at least 90% ice concentration for each region shown in Figure 1, and define $Date_{SMMR}$ using the time series of the averaged data.

Daily surface temperature fields on a 2° latitude by 10° longitude grid from 70–90° N, compiled from optimal interpolation of coastal station and drifting buoy data through the Arctic Ocean Buoy Program (AOBP) (Thorndike and Colony, 1981), are also used. Regional mean daily temperatures are computed by averaging data for all grids within each study area, with the regional melt data ($Date_{AOBP}$) defined as the first day followed by a 7-day run of mean temperatures of at least 0°C. Melt so defined should yield dates similar to those derived from the SMMR data. We are aware of potential problems in the buoy temperatures related to radiative heating during summer (Martin and Clarke, 1978). Nevertheless, the buoy fields represent the best available in situ data source.

The final data source is a five-year subset of snow-melt stages charted manually over three-day increments for the entire Arctic Ocean from May through mid-August of 1975, 1977–80 and 1984–88, based on brightness changes analyzed primarily from visible-band Defense Meteorological Satellite Program (DMSP) 2.7 km resolution orbital-swath images. The complete ten-year data set is described in detail by Robinson and others (1992).

Briefly, as the overlying winter snow cover begins to melt, there is a decrease in image brightness (as albedo decreases) and characteristic changes in surface texture due to snow becoming wet and decreasing in depth, the formation of meltponds and exposure of bare ice. Four brightness classes are identified. Typically, 15–25 images are used during each three-day charting interval, which is usually long enough to provide at least one clear-sky image over a given area, but short enough to capture temporal variations in snow melt. Surface/cloud discrimination is based on identification of cloud shadows and motion, and leads and melt ponds on the ice surface (Kukla and Robinson, 1984). Melt charts are digitized to the Limited-Area Fine Mesh version of the National Meteorological Center (NMC) grid, with open-water cells defined from Navy/NOAA ice concentration charts. Missing grid cells are filled using data from the

immediately subsequent or preceding chart (if available), usually resulting in over 80% coverage of the 223 total cells in any given chart. Only grid cells for the regions shown in Figure 1 are used here. Changes in ice concentration bias the charted classes only when concentrations are low (e.g. <75%); for the regions and times examined here, this affects only a few grid cells (Robinson and others, 1992).

Melt for a grid cell is defined using the transition from brightness class 1 to 2, which represents the first significant decrease in image brightness, and corresponds to an albedo reduction of about 15% (Robinson and others, 1992). Only ice-covered cells are considered. The timing of this transition yields a date at which melt is already well underway. The regional date of melt for each study area (defined here as $Date_{DMSP}$) is taken as the mid-point of the three-day charting interval for which all grid cells have reached at least class 2. The difference (in days) between $Date_{DMSP}$ and $Date_{SMMR}$ is taken as an index of the rate of melt progression (MP) following its earliest onset as identified in SMMR.

Cloud cover and winds

Cloud cover has been charted for May through mid-August of 1975, 1977–80 and 1984–88 for the western Arctic on a near daily basis, using 0.6 km and 2.7 km resolution DMSP imagery (Serreze and Rehder, 1990). Here, we use data for 1979, 1980, 1984–86. Clouds are differentiated from snow and ice by identification of cloud motion and characteristic features of the pack ice (cf. Kukla and Robinson, 1984). Depending on the cloud optical thickness, surface features are either partially or completely obscured. Three cloud classes are charted (cloud-free skies, thin cloud, and thick cloud) and digitized to the same NMC grid used in the DMSP snow-melt analysis. Cloudy grid cells are simply defined as those with at least 50% cloud cover. Here, we combine the thin and thick classes to provide a simple cloud/no cloud discrimination. Regional cloud characteristics for any given time period are expressed in terms of a % frequency (cloudy cells divided by total cells, multiplied by 100).

To provide a simple index of northward air advection, daily surface pressure derivatives from the AOBP, provided over the same grid as the temperature fields through optimal interpolation of a blend of buoy pressures and coastal data (see Thorndike and Colony, 1981), are used to calculate the mean meridional component (positive northward) of the surface geostrophic wind across the 70° N to 72° N latitude band over longitudes 150° W eastward to 170° E and for 170° E eastward to 130° E, giving an average meridional wind across the southern boundaries of the Beaufort and East Siberian seas, respectively (this analysis required rotation of the original *u* and *v* axes adopted in the AOBP analyses, see Thorndike and Colony, 1981).

RESULTS

Estimated melt dates for each year and region from each data set are given in Table 1, along with the correspond-

Table 1. Dates of snow melt estimated from the three data sets and their rankings (numbers in parentheses, with ties indicated by the letter T) along with the length (in days) of the melt progression (MP) interval (defined as $Date_{DMSP} - Date_{SMMR}$)

Beaufort Sea				
Year	Date _{AOBP}	Date _{SMMR}	Date _{DMSP}	MP (d)
1979	6/09 (4)	7/03 (5)	6/28 (T3)	-5
1980	6/05 (T2)	6/06 (T2)	6/28 (T3)	22
1984	6/05 (T2)	6/06 (T2)	6/13 (1)	7
1985	6/01 (1)	5/31 (1)	6/19 (2)	19
1986	6/10 (5)	6/14 (4)	6/28 (T3)	14

Year	Date _{AOBP}	Date _{SMMR}	Date _{DMSP}	MP (d)
1979	6/16 (5)	6/15 (T3)	6/25 (T2)	10
1980	6/13 (3)	6/15 (T3)	6/25 (T2)	10
1984	6/14 (4)	6/06 (2)	7/01 (T4)	25
1985	6/05 (1)	6/03 (1)	6/16 (1)	13
1986	6/09 (2)	6/15 (T3)	7/01 (T4)	16

ing MP interval. The dates are ranked from the earliest to latest year (numbers in parentheses), with ties indicated by the letter T left of the rank numbers. With one exception (see below) the DMSP analyses give the latest date of melt. This is expected, as above-freezing temperatures and the initial development of liquid water in the pack ice should occur before a significant decrease in DMSP image brightness. The values for Date_{SMMR} and Date_{AOBP} are also generally within a week of each other. The unusually late (3 July) Date_{SMMR} in 1979 for the Beaufort Sea (and hence the negative MP interval) may be spurious, as the pronounced “jump” in brightness temperatures observed in other years was poorly defined.

Date_{SMMR} for 1985 was the earliest of the five years over both the Beaufort and East Siberian seas (31 May and 3 June, respectively), with the corresponding Date_{DMSP} ranked second and first (19 June and 16 June, respectively). The MP, however, is 6 days longer in the Beaufort Sea. By comparison, while Date_{SMMR} was relatively late for both 1979 and 1980 in the East Siberian Sea (15 June), melt subsequently progressed rapidly (MP = 10 days). For 1980, this contrasts sharply with the Beaufort Sea, where the SMMR melt signal was nine days earlier than for the East Siberian Sea (6 June), but when coupled with a slightly later Date_{DMSP} leads to a long MP of 22 days. For 1984, Date_{SMMR} is again relatively early in both regions, with melt progressing rapidly in the Beaufort Sea (MP = 7 days), but much slower in the East Siberian Sea (MP = 25 days). Over the five years, the MP varies by over two weeks in both regions, with the range for both Date_{SMMR} and Date_{DMSP}

being similar. The Date_{AOBP} values show a smaller range.

To examine possible relationships between snow melt and cloud cover, Date_{SMMR} and the MP duration for each season and year are plotted against the corresponding percentage cloud frequency from 1 May to Date_{SMMR} and during the MP interval, excluding 1979 for the Beaufort Sea (discussed separately). Figure 2 shows results for Date_{SMMR} and percentage cloud frequency. While the limited size of the data sets makes a correlation analysis inappropriate, the results for the Beaufort Sea for 1984, 1985 and 1986, if considered alone, would suggest that an earlier Date_{SMMR} is associated with a lower percentage

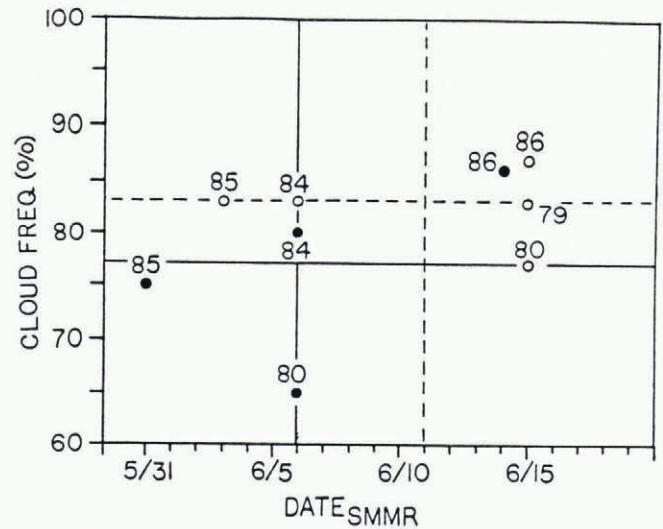


Fig. 2. Scatter plot of Date_{SMMR} versus percentage cloud frequency from 1 May to Date_{SMMR} excluding 1979 for the Beaufort Sea. Data for the Beaufort Sea are indicated by darkened circles, with open circles used for the East Siberian Sea. The year represented by each data point is also indicated. The five-year mean values (four years for the Beaufort Sea) are indicated by solid lines (Beaufort Sea) and dotted lines (East Siberian Sea).

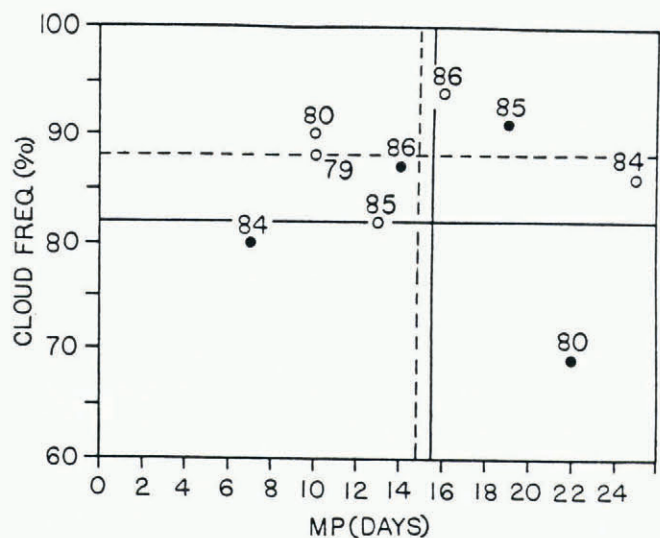


Fig. 3. Same as Figure 2, but for the MP interval versus percentage cloud frequency during the MP interval.

cloud frequency. While perhaps intuitive in terms of the effect of cloud cover on the downwelling solar flux, we would then expect that 1985, the year with earliest $Date_{SMMR}$ in both regions, rather than 1980, would also have the most limited cloud cover in both regions. Furthermore, for the East Siberian Sea, there seems to be no evidence at all for a relationship between cloud cover and $Date_{SMMR}$. Although the 3 July $Date_{SMMR}$ for 1979 in the Beaufort Sea is questionable, the corresponding cloud frequency (80%), although tied with 1984 for the second highest in this region, also offers no convincing support for a relationship between cloud cover and melt onset.

Figure 3 shows the results for percentage cloud frequency versus MP. As with the results for $Date_{SMMR}$, the MP interval shows no obvious relationship with cloud cover for either region. There is some indication for the increase in the MP duration between 1984, 1986 and 1985, respectively, in the Beaufort Sea to be related to increasing cloud cover. While by itself, this suggests that a short MP is also associated with a strong solar flux, the results for 1980 go directly counter to this argument.

Turning to northward air advection, Figure 4 shows the results for $Date_{SMMR}$ versus the mean meridional component of the geostrophic wind between 70°N to 72°N (see section above) from 1 May to $Date_{SMMR}$. For the Beaufort Sea, the results for 1985, 1984 and 1986 respectively might suggest that an earlier (later) $Date_{SMMR}$ is associated with a larger (smaller) northward wind component. The results for these three years are also consistent with the results in Table 1, showing that an earlier (later) $Date_{SMMR}$ tends to be associated with an earlier (later) date of above freezing AOBP temperatures. Comparison between Figures 2 and 4 shows that although the northward wind component

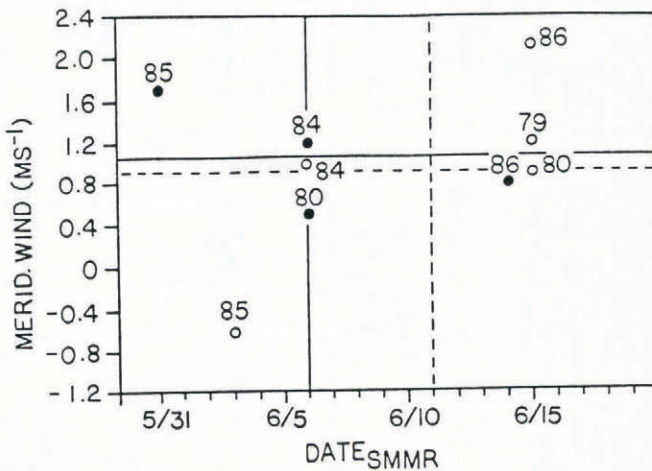


Fig. 4. Scatter plot of $Date_{SMMR}$ versus the mean meridional geostrophic wind component ($m s^{-1}$) from 1 May to $Date_{SMMR}$ excluding 1979 for the Beaufort Sea. Dates for the Beaufort Sea are indicated by darkened circles, with open circles used for the East Siberian Sea. The year represented by each data point is also indicated. The five-year mean values (four years for the Beaufort Sea) are indicated by solid lines (Beaufort Sea) and dotted lines (East Siberian Sea).

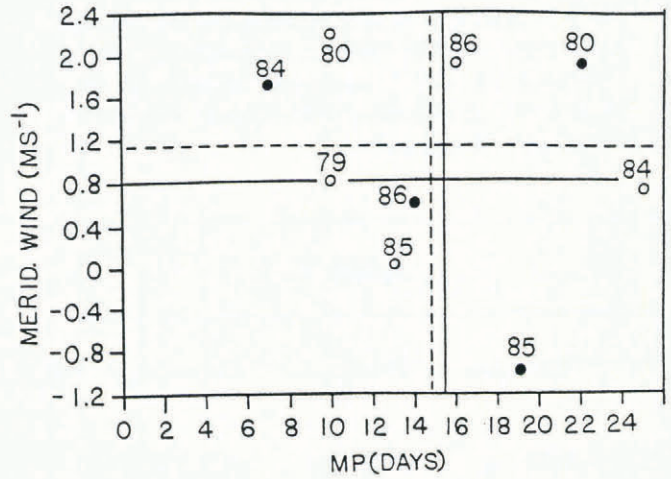


Fig. 5. Same as Figure 4, but the MP interval versus the mean meridional geostrophic wind component ($m s^{-1}$) during the MP interval.

decreased between 1985, 1984 and 1986, cloud cover increased. Based on earlier studies (e.g. Curry and Herman, 1985), an inverse association between northward winds and cloudiness would be surprising, and while perhaps only coincidental, the combination of strong northward advection and comparatively limited cloud cover, as suggested for 1985, would be very conducive to melt.

The above arguments for the Beaufort Sea, however, seem less tenable when 1980 is considered. This year had the same $Date_{SMMR}$ as for 1984, but with northward wind component of only $0.5 m s^{-1}$ associated with limited cloud cover (64%). The questionable $Date_{SMMR}$ for this region in 1979 (3 July) was associated with a small positive meridional wind ($0.6 m s^{-1}$), which, combined with comparatively extensive cloud cover (80%), might explain the late $Date_{SMMR}$. Nevertheless, at least for 1984, 1985 and 1986, the results for the East Siberian Sea suggest that stronger northward winds may be associated with a later $Date_{SMMR}$, hence further questioning the role of air advection on snow melt.

Finally, Figure 5 shows results between the mean northward wind component and the MP interval. Here, we see that the increase in the MP interval between 1984, 1986 and 1985, respectively, in the Beaufort Sea is associated with a decrease in the northward wind component. While it is again perhaps surprising that the frequency of cloud cover increased between these years (Fig. 3), the combination of strong northward advection and relatively clear skies, as suggested for 1984, would again be conducive to a short MP interval. Nevertheless, 1980 again does not fit this relationship; while also associated with strong northward winds and limited cloud cover (Fig. 3), the MP was 22 days long. Furthermore, no obvious relationships between the MP and winds are suggested for the East Siberian Sea. Attempts to relate the results in Figures 3 and 5 to average temperatures during the MP interval yield conflicting results which may, in part, reflect the biases in the buoy temperatures by solar heating near the summer solstice. Under melting conditions, surface air

temperature should remain near freezing. Nevertheless, we often observed buoy temperatures during MP intervals in excess of 5°C.

CONCLUSIONS

The use of SMMR brightness temperatures and AOBP buoy temperatures to detect the initial onset of snow melt give dates within about a week of each other, except for 1979 in the Beaufort Sea. Although the buoys are prone to solar heating (Martin and Clarke, 1978), the general agreement between the two data sets lends support to earlier studies (Anderson, 1987; Maslanik and Barry, 1989) showing that passive microwave brightness temperatures can provide a potentially useful remote-sensing tool for detecting initial snow melt over Arctic sea ice. This technique also provides a potential "early detection" strategy for identifying changes in the timing of melt related to any greenhouse-induced warming.

Our efforts to contrast interannual variations in $Date_{SMMR}$ and the MP interval with synoptic-scale forcings yield no clear relationships. There is some indication that in the Beaufort Sea, the timing of $Date_{SMMR}$ and the duration of the MP may vary in response to variations in cloud cover and air advection. In particular, the early $Date_{SMMR}$ for 1985 and the short MP for 1984 appear consistent with the combined effects of comparatively limited cloud cover and strong on ice winds. Serreze and others (1991), using anomalies in parameterized albedo based on the DMSP melt classes in conjunction with temperature anomalies at coastal stations, report relationships between early melt (low albedo) in coastal regions and on-ice airflows, which support the role of advection, but this relationship was apparent only in some years.

Years such as 1980 in the Beaufort Sea, as well as the results for all years in the East Siberian Sea, point out that other factors may mask relationships between snow melt and atmospheric forcings. One potentially significant factor is interannual variations in the depth of the initial snowpack. Furthermore, we have addressed advection simply in terms of the strength of the meridional wind, and not as sensible heat advection. Considering the sensitivity of the AOBP temperature data to radiational heating, it might be useful as a next step to examine advection using the AOBP winds in conjunction with published temperature data at coastal stations. Also with regard to data quality, the definition of $Date_{DMSP}$ is based on a subjective determination of brightness changes in the imagery. In particular, under cloudy conditions, when the surface cannot be observed, the DMSP analyses will become less accurate. The use of surface albedos derived from digital satellite data (Rossow and others, 1989) could yield a more objective method of determining surface melt (e.g., from a 20% reduction in regional albedo). Use of this technique in conjunction with SMMR brightness temperatures, or with the more recent data from the DMSP Special Sensor Microwave Imager (SSM/I), could allow synoptic controls on surface melt to be explored with greater precision.

ACKNOWLEDGEMENTS

This work was supported by NSF grant ATM 90-16563. T. Demaria is thanked for his help in cloud charting.

REFERENCES

- Ambach, W. 1974. The influence of cloudiness on the net radiation balance of a snow surface with high albedo. *J. Glaciol.*, **13**(67), 73–84.
- Anderson, M. R. 1987. The onset of spring melt in first year ice regions of the Arctic as determined from Scanning Multichannel Microwave Radiometer data for 1979 and 1980. *J. Geophys. Res.*, **92**(C12), 13,153–13,163.
- Barry, R. G., M. W. Miles, R. C. Cianflone, G. Scharfen and R. C. Schnell. 1989. Characteristics of Arctic sea ice from remote-sensing data and their relationship to atmospheric processes. *Ann. Glaciol.* **12**, 9–15.
- Curry, J. A. and G. F. Herman. 1985. Relationships between large-scale heat and moisture budgets and the occurrence of Arctic stratus clouds. *Mon. Weather Rev.*, **113**, 1441–1457.
- Kukla, G. J. and D. A. Robinson. 1984. Variability of summer cloudiness in the Arctic Basin. *Meteorol. Atmos. Phys.*, **29**, 42–50.
- Martin, P. C. and M. Clarke. 1978. A test of barometric pressure and temperature measurements from ADRAMS buoys. *AIDJEX Bull.* **40**, 61–82.
- Maslanik, J. A. and R. G. Barry. 1989. Short-term interactions between atmospheric synoptic conditions and sea ice behavior in the Arctic. *Ann. Glaciol.*, **12**, 113–117.
- Robinson, D. A., M. C. Serreze, R. G. Barry, G. Scharfen and G. Kukla. In press. Large-scale patterns and variability of snow melt and parameterized surface albedo in the Arctic Basin. *J. Climate*.
- Rosow, W. B., C. L. Brest and L. C. Gardner. 1989. Global, seasonal surface variations from satellite radiance measurements. *J. Climate*, **2**, 214–237.
- Scharfen, G., R. G. Barry, D. A. Robinson, G. Kukla and M. C. Serreze. 1987. Large-scale patterns of snow melt on Arctic sea ice mapped from meteorological satellite imagery. *Ann. Glaciol.*, **9**, 200–205.
- Serreze, M. C. and M. C. Rehder. 1990. June cloud cover over the Arctic Ocean. *Geophys. Res. Lett.*, **17**(12), 2397–2400.
- Serreze, M. C., T. L. Demaria, R. G. Barry and D. A. Robinson. 1991. Atmospheric forcings on large-scale patterns of parameterized albedo over Arctic sea ice: case studies for June 1976 and 1988. *Fifth Conference on Climate Variations, October 14–18, Denver, Colorado. Preprint volume*. Boston, MA, American Meteorological Society, 396–399.
- Thorndike, A. S. and R. Colony. 1981. *Arctic Ocean Buoy Program Data Report, 1 January 1980–31 December 1980*. Seattle, WA, University of Washington, Polar Science Center.
- Wendler, G. 1986. The "radiation paradox" on the slopes of the Antarctic continent. *Polarforschung*, **56**(1/2), 33–41.

The accuracy of references in the text and in this list is the responsibility of the authors, to whom queries should be addressed.